Anisotropic viscoelastic phase separation in polydisperse hard rods leads to nonsticky gelation

Claudia Ferreiro-Córdova[a,b,c], C. Patrick Royall[a,b,d,1], and Jeroen S. van Duijneveldt[a]

[a]School of Chemistry, University of Bristol, Bristol BS8 1TS, United Kingdom; [b]Centre for Nanoscience and Quantum Information, University of Bristol, Bristol BS8 1FD, United Kingdom; [c]Université Paris-Saclay, CNRS, Laboratoire de Physique des Solides, 91405 Orsay, France; and [d]H. H. Wills Physics Laboratory, University of Bristol, Bristol BS8 1TL, United Kingdom

Spinodal demixing into two phases having very different viscosities leads to viscoelastic networks—i.e., gels—usually as a result of attractive particle interactions. Here, however, we demonstrate demixing in a colloidal system of polydisperse, rod-like clay particles that is driven by particle repulsions instead. One of the phases is a nematic liquid crystal with a highly anisotropic viscosity, allowing flow along the director, but suppressing it in other directions. This phase coexists with a dilute isotropic phase. Real-space analysis and molecular-dynamics simulations both reveal a long-lived network structure that is locally anisotropic, yet macroscopically isotropic. We show that our system exhibits the characteristics of colloidal gelation, leading to nonsticky gels.

liquid crystals | gels | colloidal rods

Gelation, the emergence of a network of arrested material, is among the most striking everyday features of soft condensed matter (1) and is an example of viscoelastic phase separation, where a contrast in viscosity between the demixed phases leads to the formation of a long-lived network (2). Gels can be soft (and biological) materials such as proteins (3), clays (4), foods (5), hydrogels (6), and tissues (7). In addition, a more diverse range of materials, including granular matter (8), phase-demixing oxides (9), and metallic glass formers (10), also exhibit gelation.

Despite its widespread occurrence, a complete understanding of gelation remains a challenge (1). Two properties unify particulate gels produced to date. Firstly, the constituent particles experience a significant attraction to one another [which may be effective, induced, for example, by depletion effects from added polymer (11)], resulting in phase separation that arrests before completion. Secondly, with some exceptions, such as local crystallization (12), both phases are isotropic. The interparticle attraction is closely related to the phase behavior. In gelation, spinodal decomposition (immediate demixing) leads to a "colloidal liquid" phase which is of sufficient volume fraction that its high viscosity results in a long-lived network in which full demixing is suppressed (1, 2, 13, 14). Thus, colloidal gels exhibit dynamical contrast between the phases formed through spinodal decomposition (15).

Here, we depart from this paradigm of gelation driven by attraction between particles: We consider a system of polydisperse colloidal rods without significant attractions. Nevertheless, in such a system, spinodal decomposition occurs from a thermodynamically unstable isotropic fluid to an isotropic fluid in coexistence with a nematic liquid crystal (16–18).

While the phase behavior and spinodal mechanism of demixing suggests that gelation may be found, it is important to consider the dynamics: Why should the phase separation in our system arrest such that a gel forms? Now the nematic phase exhibits an anisotropic viscosity. Although the viscosity along the director is comparable to that in the isotropic phase, perpendicular to the director, the viscosity is much higher for our polydisperse system. For suitable compositions, we further-

more expect percolation of the nematic phase. We shall show that the rods align parallel to the "arms" of the gel, and, thus, while there may be flow along the arms, perpendicular flow is very strongly suppressed. We thus argue that polydisperse rods in which attraction is not important feature many of the properties required for spinodal gelation. This concept of gels formed by nematic–isotropic spinodal decomposition is shown in Fig. 1.

We identify four criteria of spinodal gelation (2). 1) The system must undergo spinodal decomposition; 2) there must be dynamic asymmetry between the phases (that is to say, one phase is substantially more viscous that the other); 3) the more viscous phase must percolate (19); and 4) the nonequilibrium nature of the gel leads to aging, in particular, coarsening.

To realize such materials, we combine real-space analysis of a colloidal model system of polydisperse hard rods with computer simulation to demonstrate the character of nonsticky gelation. Our sepiolite colloidal rods exhibit two features which are important here. Firstly, any attractions are small, as the phase diagram is consistent with that of polydisperse hard rods (20), and, as we shall show, computer simulations without any attractions exhibit the same behavior. This means that any gelation behavior we find is not attributed to attractions or even effective attractions such as those found in colloid–polymer mixtures (11). Secondly, the rods are rather polydisperse (with an effective aspect ratio $\langle L'/D' \rangle = 24.6 \pm 9.5$), leading to a large gap in

Significance

Networks of mesoscopic colloidal particles, gels, are everyday materials. Yet, our understanding of colloidal gels lags far behind their utility: Gels are out of equilibrium, so their properties change over time, often with significant consequences, such as failure of the material. However, until now, we were confident of one thing: To aggregate into a network, the colloidal particles need to attract one another. Here, we show that, in fact, colloids can form a network without significant attractions. This is surprising because particles without an attraction usually distribute themselves throughout space, rather than forming a network of particle-rich and -poor regions. Our work opens the way to "nonsticky gels" and a deeper understanding of this perplexing state of matter.

Fig. 1. (*A*) Schematic illustration of anisotropic viscoelastic phase separation. Spinodal decomposition leads to a bicontinuous network of isotropic (I) and nematic (N). *A, Inset* shows that rods align parallel to the director, indicated as n̂. We expect that the viscosity parallel to the director is low enough to permit flow, while perpendicular flow is strongly suppressed. (*B*) Snapshot of a thin slice of a simulation box of rods at $\phi = 0.140$. Colors indicate the local order parameter S_i of each rod i (*SI Appendix*) and range from dark blue (isotropic) to bright green (nematic).

volume fraction between isotropic and nematic phases at phase coexistence (Fig. 2). While this coexistence gap might shrink on long timescales due to segregation of the rods (21), this is suppressed by the slow dynamics of the nematic phase, and no evidence of segregation is seen on the experimental timescale.

The fact that the rods undergo spinodal decomposition satisfies criterion 1, and the large gap in volume fraction between isotropic and nematic phases at coexistence suggests that the latter may exhibit slow dynamics, satisfying criterion 2. Criterion 3, of percolation, also follows from spinodal decomposition; likewise, criterion 4, of aging. It is thus possible that the criteria identified for spinodal gelation are met by this system of rods, and this we go on to show.

Experimental and Simulation Methodology

Experimental System. The isotropic–nematic phase separation of colloidal suspensions of fluorescently labeled sepiolite clay par-

ticles was studied by using confocal imaging of samples with concentrations in the coexistence range. The phase diagram of our system was determined before confocal analysis, and, from this, we extracted the range of concentrations of interest. Here, we used the effective bulk rod volume fraction ϕ as a measure of the concentration, which was determined from the number density of rods and the mean rod volume. Rods were taken to be cylinders of length equal to that measured with transmission electron microscopy (TEM) plus 2δ, and diameter equal to the width measured plus 2δ. Here, $\delta = 4$ nm, the length scale of steric stabilization. The number density was determined from the mass fraction and rod mass density.

Confocal images of the system were obtained with a Leica SP5 confocal microscope using a white-light laser emitting at 500 nm. Borosilicate glass capillaries with cross-sections of 1×0.1 mm were filled with rod suspensions at effective volume fractions of $\phi = 0.021, 0.026, 0.031, 0.043, 0.054, 0.066$ and glued to microscope slides with epoxy. The samples were stirred by using a vortex mixer for 1 min before filling the capillaries. Our analysis focuses on the time evolution of the phase separation, for which we have defined $t = 0$ as the moment when the stirring stops. We presume that the vortex mixing leaves the system in an isotropic state and that $t = 0$ is the start of the demixing.

Computer Simulation. We modeled the experimental system using rods with a steep repulsive interaction. We used molecular dynamics (MD) and neglected the effect of solvent-mediated hydrodynamic interactions. Significant though these are (22), here, we chose to focus our computational resources on simulating as large a system size as possible, so that the length scales and timescales may be comparable to the experiments. Our systems consisted of up to 180,000 rods with polydispersity only in length. The length distribution of our model rods is described by a Gaussian with an average rod length of $L = 24.48\sigma \pm 9.06\sigma$. Three different global volume fractions were explored here: $\phi = 0.012$ (isotropic), $\phi = 0.145$ (coexistence), and $\phi = 0.357$ (nematic). For $\phi = 0.145$, we found a phase coexistence with
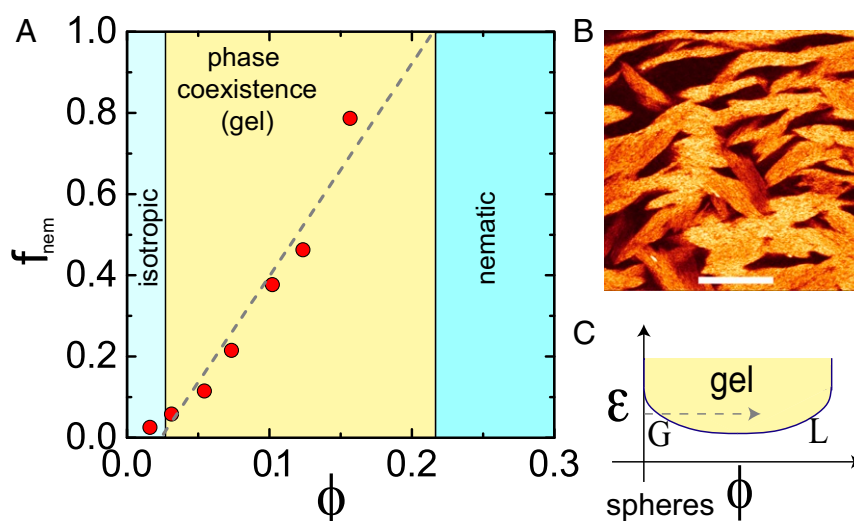
Fig. 2. Gelation via isotropic–nematic spinodal decomposition in polydisperse hard rods. (*A*) The fraction of the nematic phase f_{nem} is plotted as a function of global volume fraction ϕ. Phase coexistence occurs between $\phi_{iso}^{coex} = 0.024$ and $\phi_{nem}^{coex} = 0.215$ for the isotropic and nematic phases, respectively, and it is in this region of the phase diagram that gelation occurs (yellow shaded region). Red data points are experimental state points where we have determined f_{nem}. (*B*) Confocal image of nematic gel formed in a sample at an initial bulk volume fraction $\phi = 0.043$ for a demixing time lapse of $t = 2$ h. Bright regions indicate the nematic phase. (Scale bar, 4 μm.) (*C*) Gelation in a typical system of spheres with attraction. Shown is the phase diagram in the attraction strength ε–volume fraction ϕ plane. Here, gelation also occurs via spinodal decomposition, but this requires sufficient attraction for spinodal decomposition to a colloidal liquid (L) and gas (G). We require that the volume fraction of the colloidal liquid is sufficient to exhibit slow dynamics leading to a long-lived network. Hard spheres (without attraction $\varepsilon = 0$) do not form gels. The yellow shaded region in *A* indicates colloidal liquid–gas-phase coexistence. The dashed line indicates a path for gelation.

around 40% of the rods in a highly aligned nematic phase. The snapshots shown correspond to a system of 180,000 rods with a volume fraction $\phi = 0.140$ which corresponds to phase coexistence. Further details can be found in *Materials and Methods* and *SI Appendix*.

Nonsticky Gels of Polydisperse Rods

Our presentation of results is as follows. Firstly, we considered the phase behavior. While the isotropic–nematic transition of long rod-shaped particles has been known since the pioneering work of Onsager (23), our results show the importance of polydispersity in broadening the coexistence gap of the isotropic–nematic transition, with a nematic phase whose density is around nine times that of the isotropic phase (20). Note that the viscosity of the nematic phase varied markedly with respect to the mean rod orientation (24, 25), which has significant consequences for the behavior of the networks we obtain.

Secondly, we considered spinodal decomposition, which we demonstrate leads to a percolating network of nematic phase. We then determined the dynamical asymmetry between the isotropic and nematic phases and found the latter to be very much more viscous than the former, for flow perpendicular to the director. Finally, we considered coarsening of the network. We found behavior broadly similar to that known for spinodal gels formed of spheres (13, 15, 26), but we emphasize that the gels we obtained should exhibit flow along channels comprising the nematic phase, but that perpendicular flow should be suppressed, as our simulations showed that rods aligned parallel to the nematic domains (Fig. 1).

Phase Behavior. We present the phase diagram of our system in Fig. 2. Here, we considered the fraction of nematic phase f_{nem} as a function of (effective) volume fraction ϕ obtained from bulk observations of phase coexistence (*Materials and Methods*). The key point is that the isotropic–nematic phase coexistence was very substantially broadened due to polydispersity, as indicated in the yellow shaded region in Fig. 2. Such broadening due to polydispersity is in quantitative agreement with theoretical predictions for hard rods (21, 27). The (effective) volume fractions of the isotropic and the nematic phase in the coexistence were calculated by fitting the experimental data in Fig. 2 to a straight line. The ratio of the volume fractions at coexistence for our polydisperse system is $\phi_{\text{nem}}^{\text{coex}}/\phi_{\text{iso}}^{\text{coex}} = 0.215/0.024 = 9.00$, while that for a monodisperse system of very similar aspect ratio $L/D = 25$ is just $\phi_{\text{nem}}^{\text{coex}}/\phi_{\text{iso}}^{\text{coex}} = 0.157/0.127 = 1.22$ (28). Thus, polydispersity massively increases the density difference between the isotropic and nematic phases.

This quantitative agreement with the theoretical phase behavior for hard rods suggests that attractions are not important, but residual attractions cannot be ruled out. However, significant attractions along the length of the rods cause bundling (29, 30), while "patchy" attractions lead to the formation of a random network of rods (30). While it is hard to be certain of the absence of attractions, since either bundling or a random network would suppress the isotropic–nematic transition, the occurrence of the transition suggests that, for our system, neither effect is dominant. We therefore conclude that any attractions are weak. This is quite different from conventional gelation in spheres, where attractions drive gelation (1, 14).

A further interesting observation concerns the shape of the nematic regions, as shown in the confocal image in Fig. 2B. Here, the contrast is due to the much higher concentration of rods in the nematic compared to the isotropic phase, and the brightness levels were set such that isotropic appeared dark. Nucleating nematic droplets were expected to be elongated in shape, approximately elliptical, but with sharp ends (i.e., tactoids) (31), as has been observed in experiments on more monodisperse systems than those we consider here (32, 33). Indeed, the morphology of the bicontinuous network was consistent with tactoid-like objects having fused together. Thus, we cannot rule out the formation of tactoids and their subsequent coalescence prior to imaging. Note also that since the rod width was subresolution, we did not obtain the local director field in our experimental data.

Spinodal Decomposition. Allied with the observation of morphology distinct from that of (isolated) tactoids anticipated in the case of nucleation and growth, we found that the isotropic–nematic phase separation occurs in a spinodal-like fashion. Even at the shortest observation time accessible to our experiments (45 s from stopping vortex mixing) and at the weakest supersaturation ($\phi = 0.021$), we never observed nucleation and growth. That is to say, we did not find nucleation of nematic regions; these had always formed prior to our shortest observation time.

Gels often exhibit a bicontinuous texture. In Fig. 3A, we show a three-dimensional (3D) rendering of regions identified as nematic. We have confirmed that the regions identified as the nematic phase indeed percolate in all three dimensions and thus concluded that the percolation requirement for gelation is met. Close inspection of data such as that rendered in Fig. 3A suggests some alignment of the nematic domains. We believe this to be related to the capillary into which the sample is flowed for imaging. Such alignment may present an opportunity to produce networks whose orientation may be controlled.
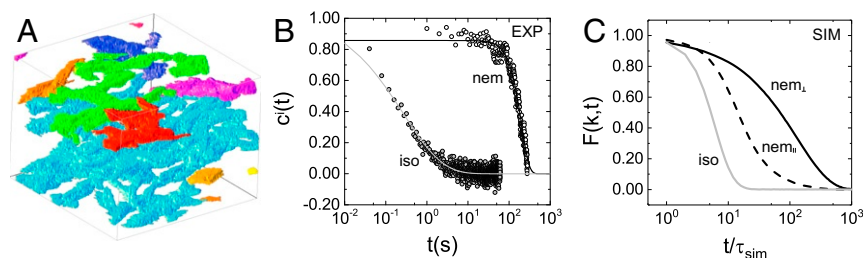
Fig. 3. Polydisperse hard rods exhibit the properties required for spinodal gelation: a percolating network and dynamic asymmetry. (A) A 3D rendering of nematic domains identified from a confocal microscopy image of a sample with a bulk effective volume fraction $\phi = 0.043$ prior to phase separation. The image corresponds to $t = 993$ s and shows a volume with dimensions of $58 \times 58 \times 35$ μm. Colors denote connected domains. The blue domain percolates the 3D image. (B) Intensity time-correlation functions for the isotropic (iso) and nematic (nem) phases. The correlation function $c(t)$ is detailed in the main text and shows that the nematic phase exhibits very much slower dynamics than does the isotropic. The lines are fits to a stretched exponential, from which we extract the relaxation time for each phase. Note that here we consider a coarse-grained description of the particle dynamics, as discussed in the text. EXP, experiment. (C) Computer simulation (SIM) data for intermediate scattering functions (which characterize particle motion). Here, we distinguish the orientation in the case of the nematic between parallel and perpendicular to the director. The wave vector $k = 0.789$ is chosen to correspond to 240 nm, which is the pixel size in the experiments. The volume fractions are $\phi = 0.012$ and $\phi = 0.36$ for the isotropic and nematic data, respectively (46).

Ferreiro-Córdova et al.

Dynamics. We now turn to the dynamical asymmetry between the phases, which is a necessary ingredient for viscoelastic phase separation, i.e., spinodal gelation (2). We shall see that our system exhibits a rather unusual form of dynamic asymmetry, due to the anisotropic dynamics of the nematic phase. In both our experiments and simulations, we measured the dynamics in a system of either isotropic or nematic phase. In this way, we probed the dynamics of the bulk phase, rather than domains in the gel network. To measure the dynamical behavior in our experiments, we used a time-correlation function $c(t)$, which measured the dynamics using pixel intensities (34). Because the width of the rods was subpixel resolution (a pixel corresponds to 240 nm), our analysis gave a coarse-grained measure of the dynamics rather than probing individual rods. In the nematic phase, where the particle separation was subresolution, a number of rods contributed to each pixel.

In Fig. 3B, we fit the time-correlation function according to a stretched exponential form $c(t) = c_0 \exp[-(t/\tau)^b]$, where c_0 and b are constants, to obtain a measure of the structural relaxation time. From our fitting, we determined relaxation times of $\tau_{iso} = 270$ ms for the isotropic and $\tau_{nem} = 202$ s for the nematic, thus indicating a considerable degree of dynamic asymmetry of three orders of magnitude. See *Materials and Methods* for further details. Our experimental data suggest that this dynamical asymmetry is comparable to the differences in dynamic properties of fast and slow phases in gels made of spheres (15).

Further insight was gained from simulation data shown in Fig. 3C, which suggest that the situation is profoundly different from the case of spheres, in which the dynamics have no preferred direction. Here, we compared the intermediate scattering function $F(k, t)$ (*SI Appendix*) at global volume fractions $\phi = 0.012$ and $\phi = 0.36$, which correspond to the isotropic and nematic phase, respectively. Note that, unlike in the experiments which considered a coarse-grained dynamics, here, we considered the particle dynamics, but at a similar length scale with respect to the rod dimensions. We saw that the dynamics of the nematic phase was such that the relaxation time perpendicular to the director was around 10 times longer than that along the director. At concentrations in the coexistence region, this led to a long-lived network of flowing channels, promoting the lifetime of the network. The main result here is qualitative: In both experiment and simulation, nematic and isotropic phases have strong dynamical contrast. Thus, we argue that three key ingredients for gelation are present: spinodal decomposition leading to a bicontinuous (percolating) network of nematic and isotropic

domains (criteria 1 and 3) and dynamical contrast between the two phases (criterion 2). By analogy to work with spheres (14), within each phase, we expected the molecular dynamics to be a reasonable description of the real dynamics. Below, we consider the time evolution (aging) of this nonequilibrium system, criterion 4.

Not all volume fractions in the simulations mapped to those in the corresponding experiments. In particular, we found the isotropic phase at somewhat higher volume fraction than in the experiments. We note that determining effective volume fractions in experiments is a challenging task (35), not to mention that the gels formed were, of course, out of equilibrium, so we would not necessarily expect a perfect mapping. We leave the accurate determination of the equilibrium phase diagram of this system to the future, noting that the network which forms is out of equilibrium and that the experiments and simulations do follow different dynamics, which can influence the network formation (36).

Coarsening. A further key feature of gels formed by spinodal decomposition is that they coarsen over time, and this is governed by the dynamics of the more viscous phase (2, 15, 26). Our system was no exception, and in Fig. 4, we present the coarsening behavior at different volume fractions in the coexistence region (*Materials and Methods*). The confocal images and 3D renderings in Fig. 4 A and B reveal structural evolution of the nematic network for $\phi = 0.043$ at $t = 149$ and 993 s from the start of the experiment. To obtain a quantitative description of coarsening, we determined a length scale from the domain size. To do this, we fit $h(r) = g(r) - 1$ with an exponential decay $h(r) = A \exp(-r/\xi)$, where A is a constant and ξ is a correlation length which measures the extent of the nematic domains. Here, $g(r)$ is the pixel-based radial distribution function (*SI Appendix*). Note that we have imposed a spherically symmetric length scale on a system of anisotropic particles. The length scales resulting from fitting of $h(r)$ are shown in Fig. 4D for a range of rod volume fractions. At early times, for our deepest quench ($\phi = 0.066$), the initial growth rate had an exponent $> 1/2$ (solid line in Fig. 4D). This is faster growth than for gels formed of spheres (15, 37), but at longer times and for weaker quenches, the growth rate was reduced, and for certain values was compatible with that of diffusive growth of $1/3$ (dashed line in Fig. 4D). We carried out a similar analysis for the simulation data at $\phi = 0.140$, which is in the coexistence region (Fig. 1B). The correlation functions $h(r)$ here were based on the correlations of the rod centers and fitted with exponentials to obtain
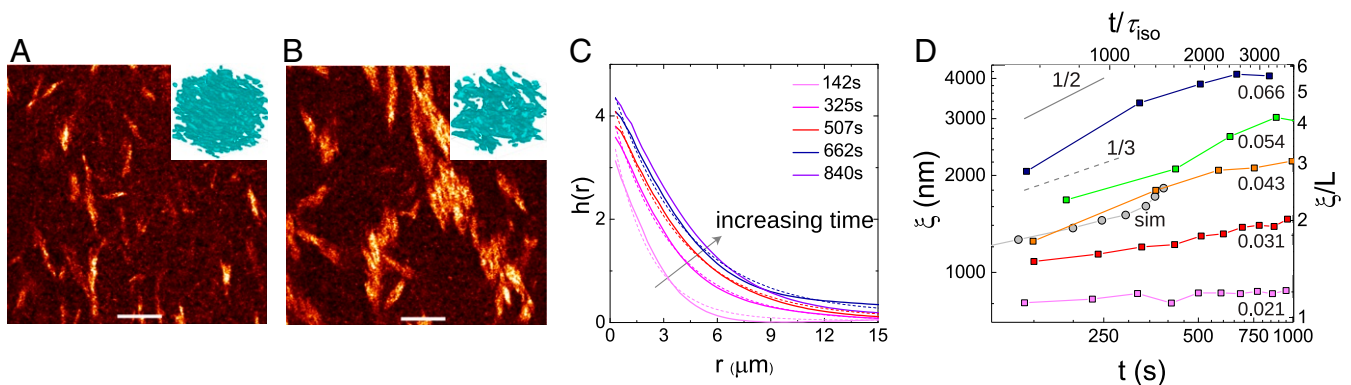
Fig. 4. Time evolution of the system. (A and B) Confocal images for a bulk volume fraction of, i.e., prior to demixing $\phi = 0.043$, at 149 s (A) and 993 s (B) showing coarsening of the network. (Scale bars, 10 µm.) A, Inset, and B, Inset correspond to 3D renderings of each sample where connectivity is clearly shown. The 3D volumes have dimensions $58 \times 58 \times 58$ µm. A, Inset, and B, Inset show renderings of the full 3D image. (C) Pair correlation functions $h(r)$ plotted at the times shown in seconds for $\phi = 0.066$ (thick solid lines). These are fitted with a decaying exponential (dashed lines) as described in the text. (D) Quantifying coarsening with the correlation length obtained from pair correlation $h(r)$ fitting. The gray solid line indicates an exponent of $1/2$ and the dashed line $1/3$, as indicated. Bulk rod volume fractions are indicated for the experimental data.

Ferreiro-Córdova et al.

a correlation length ξ. These lengths are plotted in Fig. 4D with the time scaled to the experiments by using the relaxation time in the isotropic phase τ_I to fix the timescale for both simulations and experiments. We saw very similar time evolution between the simulations and experiments. This is supportive of the idea that any residual attractions in the experimental system are unimportant; however, our choice of dynamics in the simulations may affect the rate of coarsening. Overall, the clear observation of coarsening satisfies criterion 4 for the time evolution of gels.

Conclusion and Discussion

We have argued that the properties of particulate gels, which have until now been associated with systems of attractive particles, can in fact be realized with polydisperse colloidal rods without significant attractions. By conceptual arguments, based on the dynamical contrast between the isotropic and nematic phases and spinodal demixing, we have made the case that such gels may be found in systems of rods with sufficient polydispersity, with the feature that the viscosity of the nematic network is anisotropic: Material can flow along the interior of the "arms" of the network.

This prediction we have realized using a colloidal model system of polydisperse rods of sepiolite clay. We have presented four key pieces of evidence in support of our claim, which we have supported with molecular-dynamics simulations. Firstly, the system undergoes spinodal decomposition. Secondly, the phase coexistence in these polydisperse hard rods is broad enough that the density of the nematic phase (around nine times higher than the coexisting isotropic phase) is sufficient that significant dynamic contrast between the phases is expected. We determined the dynamic contrast, with the nematic phase being much more viscous than the isotropic phase in our experiments, while our simulation data revealed strong anisotropy in the dynamics of the nematic phase. In particular, we found that the rods can readily diffuse along the director, but exhibit significant dynamic slowing perpendicular to the director. Thirdly, we have shown that the nematic phase percolates. Finally, we found coarsening behavior of the nematic domains, which is characteristic of domain coarsening in spinodal gels. We thus demonstrate a class of nonsticky gels.

We note a feature of our system distinct from gels formed of spheres. In the case of spheres, as indicated in the phase diagram of Fig. 2C, the density of the colloid-rich phase is a strong function of attraction strength, and, at high density, the dynamics of spheres is a strong function of density (15). Thus, in addition to the effects of changing the interactions between the particles, the attraction strength provides a parameter by which the density of the colloid-rich network may be controlled. In particular, one finds that moving deeper in the gel region of the phase diagram upon increasing the attraction that the rate of coarsening slows drastically, owing to the slower dynamics of the increasingly dense colloid-rich phase of spheres (2, 15).

In the case of our rods, the situation was profoundly different. In this athermal system, the rod volume fraction of the nematic phase at phase coexistence was fixed at $\phi_{\text{nem}}^{\text{coex}} = 0.215$. We see in Fig. 4 that, rather than slowing down upon moving deeper into the gel region by increasing ϕ (the global rod volume fraction), the rate of coarsening actually accelerated. We presume that this was due either to the increased thermodynamic driving force for phase separation upon increasing volume fraction or to some coupling between the dynamic anisotropy of the nematic phase and the size of the domains. It would be very interesting to explore whether the same behavior might occur in the case of spheres by moving horizontally across the gel region of the phase diagram in the (ε, ϕ) plane, as indicated by the dashed black line in Fig. 2C, rather than vertically by changing the attraction strength ε as is usually done.

It is possible to add attraction between the particles to this system by adding polymers (29). Upon adding polymer, we expect a broadening of the isotropic–nematic phase coexistence (38). Under these conditions, we expect that the gelation we observed here would be even more marked because the dynamic contrast between the phases would be even larger. This further leads to the question as to whether a more polydisperse system than those we have considered would, in fact, lead to a nematic phase with even slower dynamics than that we observed here.

A natural extension of this work is to inquire whether such behavior is restricted to rod-like particles. We expect that this nonsticky gelation may be exhibited by a variety of anisotropic particles, which exhibit a phase coexistence gap such that the viscosity of the coexisting phases is sufficiently different. The dynamic anisotropy, of course, depends on the shape of the particles, but we expect that plate-like particles may exhibit comparable behavior, if the coexistence gap between their isotropic and nematic phases is large enough. More generally, the phase behavior of a large variety of anisotropic hard particles has recently been calculated (39, 40). Determination of coexistence gaps, and particularly dynamic contrast between their coexisting phases, likely in the case of polydispersity, may show that a wide range of particle shapes exhibit nonsticky gelation.

Materials and Methods

Sample Preparation. Colloidal rod suspensions were made by using sepiolite mineral clay particles. The zeolitic water was displaced by the fluorescent dye acridine orange (41). The dye-doped particles were treated with surfactant cetyltrimethylammonium bromide solution in deionized water and centrifuged. The clay particles were dispersed in toluene and stabilized by using a polymer coating of SAP230 (Infineum). Further details can be found in *SI Appendix*.

Time-Correlation Functions. The dynamics of the system were characterized by using time sequences of xy images. The time-resolved correlation technique (34) was used in images at t' and $t' + t$ values, where t represents the time over which the correlation is made. This technique measures the change in configuration by calculating the degree of correlation in the images. This correlation is calculated using individual pixel intensity values $I(\mathbf{r}, t)$ of the images captured and can be written as

$$C^i(t, t') = \frac{\langle I(\mathbf{r}, t')I(\mathbf{r}, t' + t)\rangle_{\text{pix}}}{\langle I(\mathbf{r}, t')\rangle_{\text{pix}}\langle I(\mathbf{r}, t' + t)\rangle_{\text{pix}}} - 1. \qquad [1]$$

$\langle \rangle_{\text{pix}}$ indicates average over all of the pixels in the image. The correlation index $C^i(t, t')$ can be normalized as $c(t, t') = C^i(t, t')/C^i(0, t')$ to obtain a measurement of the relaxation time in each phase.

To obtain fully demixed isotropic and nematic phases, a suspension in the coexistence regime was allowed to phase separate in a capillary for 48 h. This compares to the timescale of the gel, which is several hours. Each phase was imaged far from the interface and the walls of the capillary. Two different time steps τ were chosen: 0.020 s for the isotropic phase and 1.0 s for the nematic phase. The data in Fig. 3B have been corrected to account for noise in the intensity measured with the confocal microscope. This was made by normalizing the $c(t)$ values obtained with the first point in the correlation curve. To make the dynamic contrast clear, we subtracted the constant value that $c(t \to \infty)$ approaches at long times, prior to the fitting in Fig. 3B. The pixel size of the images used was close to 240 nm, around eight times the rod diameter. This set the length scale over which the dynamics were probed in Fig. 3B.

Computer Simulations. We modeled our colloidal rods as linear rigid bodies composed of a number of spheres of mass m that interact only with the spheres of neighboring rods via a Weeks–Chandler–Andersen potential,

$$u_{\text{WCA}}(r) = \begin{cases} 4\epsilon\left[\left(\frac{\sigma}{r}\right)^{12} - \left(\frac{\sigma}{r}\right)^6\right] + \epsilon & r < 2^{1/6}\sigma, \\ 0 & r \geq 2^{1/6}\sigma, \end{cases} \qquad [2]$$

where r is the center-of-mass distance between two spheres, σ is the approximated diameter of the repulsive core, and ϵ is the strength of the interaction in units of $k_B T$. For simplicity, we have set $\epsilon = 1$ and $\sigma = 1$ and

the unit of time $\tau_{\text{sim}} = \sqrt{m\sigma^2/k_BT}$. Two spheres were used for each rod segment of length 1σ, giving a total of 3,117,060 spheres for the small box of 65,000 rods and 8,632,884 spheres for the large box of 180,000 rods. The volume fractions were calculated by modeling the rods as hard spherocylinders with diameter $D = \sigma = 1$ to approximate the hard core.

For our simulations, we used the open-source MD simulation package LAMMPS (42), which has a dynamical integrator for rigid bodies (43, 44). To simulate our experimental conditions, we first equilibrated a system of polydisperse rods at a low volume fraction ($\phi < 0.01$) in a constant number, volume, and temperature (NVT) ensemble using a Nóse–Hoover thermostat with chains (45). After this, a constant number, pressure, and temperature ensemble with a Nóse–Hoover barostat and thermostat with chains was used to reach the desired concentrations. A final production run was carried out in an NVT ensemble. Two simulation time steps were used. For the sample preparation up to the desired volume fraction, the time step was fixed to $\delta t = 0.001\ \tau_{\text{sim}}$. The production run was carried out by using $\delta t = 0.005\ \tau_{\text{sim}}$. Total simulation times were of $2 \times 10^4\ \tau_{\text{sim}}$ to $6 \times 10^4\ \tau_{\text{sim}}$,

depending on the box size and packing fraction. Periodic boundary conditions were applied. All data plotted in this work can be downloaded from ref. 46.

1. E. Zaccarelli, Colloidal gels: Equilibrium and non-equilibrium routes. *J. Phys. Condens. Matter* **19**, 323101 (2007).
2. H. Tanaka, Viscoelastic phase separation. *J. Phys. Condens. Matter* **12**, R207 (2000).
3. F. Cardinaux, T. Gibaud, A. Stradner, P. Schurtenberger, Interplay between spinodal decomposition and glass formation in proteins exhibiting short-range attractions. *Phys. Rev. Lett.* **99**, 118301 (2007).
4. S. Jabbari-Farouji, G. Wegdam, D. Bonn, Gels and glasses in a single system: Evidence for an intricate free-energy landscape of glassy materials. *Phys. Rev. Lett.* **99**, 065701 (2007).
5. H. Tanaka, Viscoelastic phase separation in soft matter and foods. *Faraday Discuss* **167**, 9–76 (2013).
6. M. E. Helgeson, S. E. Moran, H. Z. An, P. S. Doyle, Mesoporous organohydrogels from thermogelling photocrosslinkable nanoemulsions. *Nat. Mater.* **11**, 344–352 (2012).
7. S. Rose *et al.*, Nanoparticle solutions as adhesives for gels and biological tissues. *Nature* **505**, 382–385 (2014).
8. S. Ulrich *et al.*, Cooling and aggregation in wet granulates. *Phys. Rev. Lett.* **102**, 148002 (2009).
9. D. Bouttes, E. Gouillart, E. Boller, D. Dalmas, D. Vandembroucq, Fragmentation and limits to dynamical scaling in viscous coarsening: An interrupted in situ X-ray tomographic study. *Phys. Rev. Lett.* **112**, 245701 (2014).
10. R. E. Baumer, M. J. Demkowicz, Glass transition by gelation in a phase separating binary alloy. *Phys. Rev. Lett.* **110**, 145502 (2013).
11. W. C. K. Poon, The physics of a model colloid-polymer mixture. *J. Phys. Condens. Matter* **14**, R859–R880 (2002).
12. T. H. Zhang, J. Klok, R. H. Tromp, J. Groenewold, W. K. Kegel, Non-equilibrium cluster states in colloids with competing interactions. *Soft Matter* **8**, 667–672 (2012).
13. P. J. Lu *et al.*, Gelation of particles with short-range attraction. *Nature* **453**, 499–504 (2008).
14. C. P. Royall, S. R. Williams, H. Tanaka, Vitrification and gelation in sticky spheres. *J. Chem. Phys.* **148**, 044501 (2018).
15. I. Zhang, C. P. Royall, M. A. Faers, P. Bartlett, Phase separation dynamics in colloid-polymer mixtures: The effect of interaction range. *Soft Matter* **9**, 2076–2084 (2013).
16. M. P. B. van Bruggen, J. K. G. Dhont, H. N. W. Lekkerkerker, Morphology and kinetics of the isotropic-nematic phase transition in dispersions of hard rods. *Macromolecules* **32**, 2256–2264 (1999).
17. R. Ni, S. Belli, R. van Roij, M. Dijkstra, Glassy dynamics, spinodal fluctuations, and the kinetic limit of nucleation in suspensions of colloidal hard rods. *Phys. Rev. Lett.* **105**, 088302 (2010).
18. M. P. Lettinga *et al.*, Nematic-isotropic spinodal decomposition kinetics of rodlike viruses. *Phys. Rev. E* **73**, 011412 (2006).
19. M. E. Cates, M. Fuchs, K. Kroy, W. C. K. Poon, A. M. Puertas, Theory and simulation of gelation, arrest and yielding in attracting colloids. *J. Phys. Condens. Matter* **16**, S4861 (2004).
20. P. Woolston, J. S. van Duijneveldt, Isotropic-nematic phase transition of polydisperse clay rods. *J. Chem. Phys.* **142**, 184901 (2015).
21. A. Speranza, P. Sollich, Simplified Onsager theory for isotropic-nematic phase equilibria of length polydisperse hard rods. *J. Chem. Phys.* **117**, 5421–5436 (2002).
22. M. P. Lettinga, J. K. G. Dhont, Z. Zhang, S. Messlinger, G. Gompper, Hydrodynamic interactions in rod suspensions with orientational ordering. *Soft Matter* **6**, 4556–4562 (2010).
23. L. Onsager, The effects of shape on the interaction of colloidal particles. *Ann. N. Y. Acad. Sci.* **51**, 627–659 (1949).
24. M. P. Allen, Diffusion coefficient increases with density in hard ellipsoid liquid crystals. *Phys. Rev. Lett.* **65**, 2881–2884 (1990).
25. M. P. B. van Bruggen, H. N. W. Lekkerkerker, G. Maret, J. K. G. Dhont, Long-time translational self-diffusion in isotropic and nematic dispersions of colloidal rods. *Phys. Rev. E* **58**, 7668–7677 (1998).
26. V. Testard, L. Bethier, W. Kob, Intermittent dynamics and logarithmic domain growth during the spinodal decomposition of a glass-forming liquid. *J. Chem. Phys.* **140**, 164502 (2014).
27. H. H. Wensink, G. J. Vroege, Isotropic-nematic phase behavior of length-polydisperse hard rods. *J. Chem. Phys.* **119**, 6868–6882 (2003).
28. P. Bolhuis, D. Frenkel, Tracing the phase boundaries of hard spherocylinders. *J. Chem. Phys.* **106**, 666–687 (1997).
29. G. M. H. Wilkins, P. T. Spicer, M. J. Solomon, Colloidal system to explore structural and dynamical transitions in rod networks, gels, and glasses. *Langmuir* **25**, 8951–8959 (2009).
30. N. Kazem, M. Carmel, C. E. Maloney, Gelation and mechanical response of patchy rods. *Soft Matter* **11**, 7877–7887 (2015).
31. P. Prinsen, P. van der Schoot, Shape and director-field transformation of tactoids. *Phys. Rev. E* **68**, 021701 (2003).
32. P. W. Oakes, J. Viamontes, J. X. Tang, Growth of tactoidal droplets during the first-order isotropic to nematic phase transition of F-actin. *Phys. Rev. E* **75**, 061902 (2007).
33. N. Puech, E. Grelet, P. Poulin, C. Blanc, P. van der Schoot, Nematic droplets in aqueous dispersions of carbon nanotubes. *Phys. Rev. E* **82**, 020702 (2010).
34. S. Buzzaccaro, M. D. Alaimo, E. Secchi, R. Piazza, Spatially-resolved heterogeneous dynamics in a strong colloidal gel. *J. Phys. Condens. Matter* **27**, 194120 (2015).
35. C. P. Royall, W. C. K. Poon, E. R. Weeks, In search of colloidal hard spheres. *Soft Matter* **9**, 17–27 (2013).
36. C. P. Royall, J. Eggers, A. Furukawa, H. Tanaka, Probing colloidal gels at multiple length scales: The role of hydrodynamics. *Phys. Rev. Lett.* **114**, 258302 (2015).
37. V. Testard, L. Berthier, W. Kob, Influence of the glass transition on the liquid-gas spinodal decomposition. *Phys. Rev. Lett.* **106**, 125702 (2011).
38. R. Tuinier, T. Taniguchi, H. Wensink, Phase behavior of a suspension of hard spherocylinders plus ideal polymer chains. *Eur. Phys. J. E.* **23**, 355–365 (2007).
39. P. F. Damasceno, M. Engel, S. C. Glotzer, Predictive self-assembly of polyhedra into complex structures. *Science* **337**, 453–457 (2012).
40. M. Dijkstra, Entropy-driven phase transitions in colloids: From spheres to anisotropic particles. *Adv. Chem. Phys.* **156**, 35–71 (2014).
41. N. Yasarawan, J. S. van Duijneveldt, Arrested phase separation of colloidal rod-sphere mixtures. *Soft Matter* **6**, 353–362 (2010).
42. S. Plimpton, Fast parallel algorithms for short-range molecular dynamics. *J. Comput. Phys.* **117**, 1–19 (1995).
43. T. F. Miller *et al.*, Symplectic quaternion scheme for biophysical molecular dynamics. *J. Chem. Phys.* **116**, 8649–8659 (2002).
44. H. Kamberaj, R. Low, M. Neal, Time reversible and symplectic integrators for molecular dynamics simulations of rigid molecules. *J. Chem. Phys.* **122**, 224114 (2005).
45. G. J. Martyna, M. L. Klein, M. Tuckerman, Nosé–Hoover chains: The canonical ensemble via continuous dynamics. *J. Chem. Phys.* **97**, 2635–2643 (1992).
46. C. Ferreiro-Cordova, C. P. Royall, J. S. van Duijneveldt, Data from "Anisotropic viscoelastic phase separation in polydisperse hard rods: Non-sticky gelation." University of Bristol Research Data Repository. https://doi.org/10.5523/bris. 1gfhyy3l2qipg2t8wg6t6f1c0k. Deposited 11 January 2020.

Ferreiro-Córdova et al.